



ELSEVIER

Contents lists available at ScienceDirect

International Journal of Heat and Mass Transfer

journal homepage: www.elsevier.com/locate/hmt

Analytical fractal models for permeability and conductivity of open-cell metallic foams

Tian Xiao^a, Xiaohu Yang^{b,*}, Kamel Hooman^c, Tian Jian Lu^{d,e,*}

^aState Key Laboratory for Strength and Vibration of Mechanical Structures, School of Aerospace, Xi'an Jiaotong University, Xi'an 710049, China

^bInstitute of the Building Environment & Sustainability Technology, School of Human Settlements and Civil Engineering, Xi'an Jiaotong University, Xi'an 710049, P.R. China

^cSchool of Mechanical and Mining Engineering, The University of Queensland, Brisbane, QLD 4072, Australia

^dState Key Laboratory of Mechanics and Control of Mechanical Structures, Nanjing University of Aeronautics and Astronautics, Nanjing 210016, P.R. China

^eMIT key Laboratory of Multifunctional Lightweight Materials and Structures (MLMS), Nanjing University of Aeronautics and Astronautics, Nanjing 210016, P.R. China

ARTICLE INFO

Article history:

Received 11 January 2021

Revised 7 May 2021

Accepted 17 May 2021

Available online 13 June 2021

Keywords:

Permeability

Effective thermal conductivity

Fractal analysis

Open-cell foam

ABSTRACT

It is demonstrated that analytical models of permeability and effective thermal conductivity for open-cell metallic foams can be developed using fractal theory, for the theory lends itself better to the problem at hand where the pore morphology of the foam is typically random. Upon determining the average tortuosity based on selected representative flow streamlines in a representative structure (RS) of the foam, the permeability as a function of porosity, average tortuosity and pore size ratio is analytically obtained, with no empirical or fitting parameter needed. Similarly, the analytical fractal model of effective thermal conductivity does not include any empirical or fitting parameter. Good agreement with experimental data verifies both models, squarely justifying the applicability of using fractal theory to characterize open-cell metallic foams. It is also demonstrated that the present fractal models can better characterize the randomness of pore distributions than previous permeability and conductivity models built upon simplified geometries including periodically distributed unit cells.

© 2021 Elsevier Ltd. All rights reserved.

1. Introduction

With attributes like high porosity, ultra-low density, high specific area and fluid blending capability, open-cell metallic foams have been widely involved in a broad range of engineering applications [1-5] such as thermal management of electronics devices, thermal energy storage, chemical catalyst, fuel cells, porous burner, refrigeration, volumetric solar receiver, and biomedical applications. For such applications, permeability and thermal conductivity of the porous metals are key parameters. Macroscopically, characterization of permeability and conductivity serves the basis for utilizing metal foams since they quantitatively justify fluid and thermal transport in a porous medium. Microscopically, it is essential to get in-depth understanding on the relevant transport phenomena in porous media at pore scale.

Since metallic foams are consisted of randomly-distributed solid ligaments that form inter-connected pore space, directly solving the Navier-Stokes equations to obtain permeability or solving the

Laplace heat conduction equations to achieve thermal conductivity seem impossible. For simplification, the complicated porous structure is often assumed to be periodically distributed. Unit cells (UCs) or part of the UC are typically selected to represent both the topological and morphological features of a bulk porous medium. Based upon UC selection, two common methods have been proposed to determine the permeability and conductivity of open-celled metallic foam. On the one hand, its randomly-distributed structure was modelled as packed spheres, thus enabling calculating its permeability via modifying the Kozeny-Carmen equation [6] and its conductivity by extending the Maxwell-Eucken equation [7]. Although satisfactory agreement could be obtained thanks to the fitting empirical constants for either permeability or conductivity, there were empirical constants in the equations of the Kozeny-Carmen model for permeability and the Maxwell-Eucken model for conductivity; these empirical constants were also different for different porous media. Besides, the UC of packed spheres seemed inappropriate for representing the cellular matrix of open-celled metal foam, for transport physics between the two types of porous medium was significantly different. On the other hand, to better represent the porous structure of metal foam, a periodically-distributed cubic lattice truss was selected as the UC. The method

* Corresponding author.

E-mail addresses: xiaohuyang@xjtu.edu.cn (X. Yang), tjlu@nuaa.edu.cn (T.J. Lu).

Nomenclature

Symbols

a	Weight value
C	Empirical parameters
d	Microscopic length scale (m)
d_E	Euclidean dimension
d_s	Ligament thickness (m)
d_p	Pore diameter of representative structure (m)
D_f	Fractal dimension of the pore size distribution
D_T	Fractal dimension of the average tortuosity
G	Geometric shape factor
k	Thermal conductivity (W/m-K)
K	Permeability (m ²)
l	Length (m)
L_0	Characteristic length (m)
P	Perimeter of the cross section (m)
S	Area of the cross section (m ²)
V	Volume (m ³)
V_{total}	Total of volume (m ³)
V_{pore}	Pore of volume (m ³)

Greek symbols

μ	Dynamic viscosity (Pa · s)
λ	Pore diameter (m)
ε	Porosity
τ	Tortuosity
γ	Dimensionless number

Subscript

av	Average
e	Effective
exp	Experiment
f	Fluid
max	Maximum
min	Minimum
pre	Prediction
RS	Representative structure
s	Solid
t	Total

of volume-averaging was thence used to solve the Hagen-Poiseuille flow in the cubic UC for permeability [8], while the thermal resistance network model was employed for modelling heat conduction in the UC [9]. Although these efforts based upon packed spheres, cubic lattices [10] and polyhedrons [11-15] were undertaken to understand and predict the permeability and effective conductivity of open-celled metal foams, the assumptions made thereof were too ideal to account for the randomness of pore structure typically found in these porous metals. It is therefore envisioned that a new model that can better represent the factual randomness of pore size and distribution in metal foams is needed.

It has been established that fractal theory can describe and characterize porous media with randomly-distributed pores [16], such as metal foams, Sierpinski structures, fibrous materials, soil, oil/gas reservoir, etc. Therefore, given that the pore structure and distribution in open-cell metallic foams are random, the problem of disorderly arranged pores and tortuous flow at pore scale may be solved with the fractal theory to predict the permeability and effective thermal conductivity.

For permeability modelling, fractal distribution of capillaries was firstly applied to a capillary bundle model to develop an analytical formulas of permeable flow in bi-dispersed porous medium [17], which inspired subsequent studies on permeable transport flow in fractal porous media. Subsequent theoretical studies con-

tinuously contributed to the development of permeable flow in fractal porous materials. Correspondingly, effects of fractal porosity and pore volume distribution, tortuosity, maximum pore size, size distribution of contact areas and surface roughness on fluid transport and permeability for various kinds of porous media were quantified, as summarized in recent reviews [18].

For conductivity modelling, the fractal theory provides an altered methodology to estimate the effective thermal conductivity of porous materials with random pore sizes and distributions [19], such as porous rocks, particle porous media and fibrous materials. For typical instance, the geometric percolation model was incorporated into the fractal theory to thermal transport in porous media, thus enabling expressing the effective conductivity as a function of porosity and microstructural parameters. Nonetheless, the fractal theory is yet used to analytically calculate the effective thermal conductivity of open-cell metal foams.

To be conclusive, previous investigations contributed to the development of fractal theory on understanding thermal and fluid transport phenomena in porous media and predicting their permeability and conductivity. However, little attention has been paid to specific fractal considerations of the micro pore structures of open-cell foams and the validity of using fractal theory to develop permeability and conductivity models for open-cell foams against experimental measurements. Besides, justification of the predicted contribution of micro pore structure to flow features inside open-cell metal foams using fractal theory remains elusive. This paper follows the basis assumption of isotropic microstructure for metal foam proposed by previous studies [12, 20], the anisotropy effects [21, 22] caused by cell elongations that make significant contribution to the fluid flow and heat conduction are not considered in the current study. To this end, in the current study based on the isotropic assumption, pore-scale geometric characterization was performed for open-cell metallic foams, which was then employed to construct analytical fractal models for permeability as well as effective thermal conductivity. Subsequently, model estimations were compared with existing experimental data of permeability and conductivity for a wide variety range of open-cell metallic foams. Finally, the models were employed to quantify the variation of pressure drop with porosity as well as the effects of metal foam materials and filling fluids on effective thermal conductivity.

2. Theoretical model

2.1. Theory for fractal porous media

Cumulative size distribution of pores in a porous medium or spots on an engineering surface follows typically a fractal scaling law [23]. Thus, in the theory of fractal geometry, the measure of a fractal object $M(l)$ and the measurement scale l obey the following scaling law [23]:

$$M(l) \propto l^{D_f} \quad (1)$$

where D_f is the fractal dimension of the fractal object. Consequently, for a porous medium such as open-cell metal foam, the fractal scaling law between the number N of pores and the pore size λ can be expressed as [17]:

$$N(l \geq \lambda) = (\lambda_{max}/\lambda)^{D_f} \quad (2)$$

where λ_{max} denotes the maximum pore size and $N(l \geq \lambda)$ represents the total number of pores having sizes no less than λ . Upon replacing λ with the minimum pore diameter λ_{min} , the total number N_t of pores can be obtained as [17]:

$$N_t(l \geq \lambda_{min}) = (\lambda_{max}/\lambda_{min})^{D_f} \quad (3)$$

Upon differentiating λ in Eq. (2), the number of pores in the infinitesimal range of λ to $\lambda + d\lambda$ can be obtained as [24]:

$$-dN = D_f \lambda_{\max}^{D_f} \lambda^{-(D_f+1)} d\lambda \quad (4)$$

Dividing Eq. (4) by Eq. (3) gives further:

$$-\frac{dN}{N_t} = D_f \lambda_{\min}^{D_f} \lambda^{-(D_f+1)} d\lambda = f(\lambda) d\lambda \quad (5)$$

where $f(\lambda) = D_f \lambda_{\min}^{D_f} \lambda^{-(D_f+1)}$ is the probability density function of pores in the fractal porous medium [16, 17]. According to the theory of probability, the integral of probability density function exhibits the following relationship [16, 17]:

$$\int_{-\infty}^{+\infty} f(\lambda) d\lambda = \int_{\lambda_{\min}}^{\lambda_{\max}} f(\lambda) d\lambda = 1 - \left(\frac{\lambda_{\min}}{\lambda_{\max}}\right)^{D_f} \equiv 1 \quad (6)$$

if and only if:

$$\left(\frac{\lambda_{\min}}{\lambda_{\max}}\right)^{D_f} \cong 0 \quad (7)$$

It has been suggested [16] that using the relationship of Eq. (6) is a key step for employing the theory of fractal geometry to deal with porous media. For instance, based on the Sierpinski carpet and the Sierpinski sponge model, analytical expressions of fractal dimensions could be derived from Eq. (6) [16].

Equations (1) to (7) lay the theoretical basis of fractal geometry for porous media.

2.2. Fractal model of permeability

With tortuous flow in a porous medium modelled as flow inside a bundle of tortuous circular capillary tubes having circular cross-sections, a fractal model of permeability had been proposed [17], as:

$$K = \frac{\pi}{128} \frac{L_0^{-1-D_T} D_f}{3 + D_T - D_f} \lambda_{\max}^{3+D_T} \quad (8)$$

where L_0 is the characteristic length containing all fractal pores (from the smallest to the largest size) of the porous medium, D_T is the fractal dimension of average tortuosity, λ_{\max} is the maximum pore diameter, and D_f denotes the fractal dimension of pore size distribution. For two-dimensional space, $1 < D_f < 2$; for three-dimensional space, $2 < D_f < 3$. An expression for D_f as was further proposed as [16]:

$$D_f = d_E - \frac{\ln \varepsilon}{\ln(\lambda_{\min}/\lambda_{\max})} \quad (9)$$

where λ_{\min} is the minimum pore diameter, ε is the porosity, and d_E is the Euclidean dimension, e.g., $d_E = 2, 3$ are the two- and three-dimensional space, in respective.

As the model of Eq. (8) is yet proven to be applicable for predicting the permeability of open-cell metal foams, its key parameters (L_0 , D_T , λ_{\max} and G) are determined below for high-porosity metallic foams having open cells.

2.2.1. Characteristic length L_0

Fig. 1(a) and (b) depict both optical (low magnification) and scanning electronic microscopic (SEM) images for a high porosity, open-cell aluminum foam. Both large and small pores are observed, especially from the SEM image of Fig. 1(b), and these pores are randomly distributed, in accordance with the fundamental assumption of fractal theory. In the current study, for simplicity, the irregular pores are assumed to be cubic with random sizes, as shown in Fig. 1(c). Out of the disordered cubic pores, the joint with three struts is selected as the representative structure (RS) for subsequent characterization analysis. With reference to Fig. 1(d),

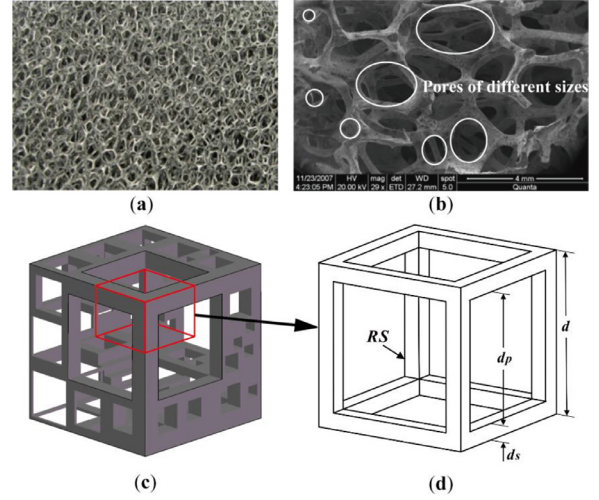


Fig. 1. High porosity open-cell aluminum foam: (a) cellular morphology [20]; (b) scanning electronic microscope (SEM) image [20]; (c) idealized cubic representation for random pore structure and distribution; (d) representative structure (RS) for open-cell metal foams

let d , d_p and d_s represent separately the microscopic length scale, the pore size and the ligament thickness of the RS.

The characteristic length L_0 characterizes a size scale in which all the fractal pores, from smallest to largest size, are contained. Within the length scale, the porosity of the foam with length L_0 can be calculated as:

$$\varepsilon = \frac{V_{pore}}{L_0^3} \quad (10)$$

where V_{pore} is the volume of all the pores in the foam. For a high porosity open-cell metallic foam, its pores typically exhibit a shape close to dodecahedron or tetrahedron [25]. Therefore, to simplify the current calculation, the pores are idealized as spherical ones. The total pore volume may then be calculated as [26]:

$$V_{pore} = \frac{\pi D_{f,3} \lambda_{\max}^3}{6(3 - D_{f,3})} (1 - \varepsilon) \quad (11)$$

where $D_{f,3} = 3 - \frac{\ln \varepsilon}{\ln(\lambda_{\min}/\lambda_{\max})}$. According to Eqs. (10) and (11), the characteristic length L_0 can be obtained as:

$$L_0 = \lambda_{\max} \left[\frac{\pi D_{f,3}}{6(3 - D_{f,3})} \frac{1 - \varepsilon}{\varepsilon} \right]^{\frac{1}{3}} \quad (12)$$

The pores in the cubic structure of Fig. 1(c) may be considered as squares with varying size (λ), such that the total pore area A_p may be calculated as:

$$A_p = - \int_{\lambda_{\min}}^{\lambda_{\max}} \lambda^2 dN = \frac{D_{f,2} \lambda_{\max}^2}{(2 - D_{f,2})} (1 - \varepsilon) \quad (13)$$

where $D_{f,2} = 2 - \frac{\ln \varepsilon}{\ln(\lambda_{\min}/\lambda_{\max})}$. It follows that the total cross-sectional area of the foam is given by:

$$A = \frac{A_p}{\varepsilon} = \frac{D_{f,2} \lambda_{\max}^2 (1 - \varepsilon)}{(2 - D_{f,2}) \varepsilon} \quad (14)$$

2.2.2. Fractal dimension of average tortuosity, D_T

With the tortuous path of fluid through a porous medium (e.g., cellular foam) approximately viewed as a bundle of tortuous capillary tubes, an analytical method for determining the fractal dimension of average tortuosity D_T had been proposed [27], yielding:

$$D_T = 1 + \frac{\ln \tau_{av}}{\ln(L_0/\lambda_{av})} \quad (15)$$

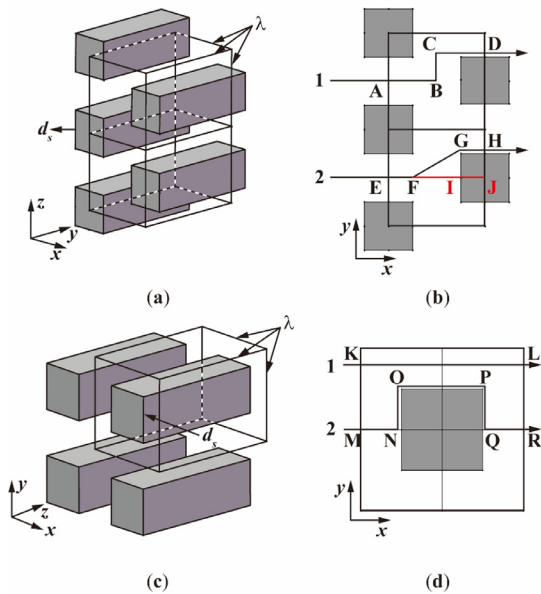


Fig. 2. Distribution of streamlines as seen from different angles of view: (a) three-dimensional configuration for square ligaments in a dislocated and equidistant arrangement and the corresponding unit cell; (b) side view of streamlines flowing around square ligaments in a dislocated and equidistant arrangement; (c) three-dimensional configuration for square ligament in a square arrangement and the corresponding unit cell; (d) side view of streamlines flowing around square ligaments in a square arrangement

where λ_{av} and τ_{av} are the average pore diameter and the average tortuosity, respectively. While $D_T = 1$ represents a straight channel/tube, $D_T = 3$ represents a tortuous channel/tube filling a three-dimensional space. For a three-dimensional porous medium, $1 < D_T < 3$.

With fractal theory, the average pore diameter of the foam is calculated as [27]:

$$\lambda_{av} = \frac{D_{f,3} \lambda_{\min}}{D_{f,3} - 1} \quad (16)$$

Once $D_{f,3}$ and L_0 are determined, the only key parameter yet to characterize is the average tortuosity τ_{av} . The tortuosity of a porous medium is defined as the ratio of the length for a real tortuous flow path to the that of a straight (minimal) one [28], thus accounting for the elongation extent of flow path. As numerous streamlines are present within a porous medium like cellular metallic foam, it had been demonstrated that the average tortuosity could be estimated as the average of representative streamlines [29]. Fig. 2 depicts the distribution of streamlines in the cubic RS. Two representative structures of ligaments distribution are selected, as shown in Fig. 2(a) and (c). Since the open-cell foam is composed of random-sized pores, some ligaments are dislocated. Accordingly, both the dislocated and equidistant ligaments are used to calculate the tortuosity, as illustrated in Fig. 2(a). To further simplify the calculation, the irregular pore structures are simplified into cubic representative structures: correspondingly, the ligaments distributed in a square arrangement are used to calculate the tortuosity, as depicted in Fig. 2(c).

For open-cell metal foams with idealized pore structures, the average tortuosity is obtained using a weighted average over all possible streamlines around two representative ligament arrangements, as shown in Fig. 2(b) and (d), as:

$$\tau_{av} = \sum_{i=1}^n a_i \tau_i \quad (17)$$

where n is the total number of possible streamlines, a is the weight value ($\sum_{i=1}^n a_i = 1$), and τ_i is the tortuosity of the i -th flow streamline. When $a_1 = a_2 = \dots = a_n$, Eq. (17) is reduced to a simple statistical average [29]. Given that numerous flow paths exist in a RS, it seems not possible to find and calculate all path lines of fluid flow to finalize the average tortuosity. It was suggested [29] that the average tortuosity is related to the averaged tortuosity for two representative flow paths: the longest and the shortest. The length, width and height of the representative structure as shown in Fig. 2(a) and (c) are d . Therefore, the total pore volume in the representative structure can be calculated by:

$$V_{RS-pore} = \lambda^3 - \lambda \cdot d_s^2 \quad (18)$$

where d_s is the side length of the square ligament, and the total volume of the cubic representative structure is:

$$V_{RS-total} = \lambda^3 \quad (19)$$

Therefore, for the structures of Fig. 2(a) and (c), the porosity is:

$$\varepsilon = \frac{V_{RS-pore}}{V_{RS-total}} = 1 - \left(\frac{d_s}{\lambda}\right)^2 \quad (20)$$

It follows that:

$$\frac{d_s}{\lambda} = \sqrt{1 - \varepsilon} \quad (21)$$

For streamline 1 in Fig. 2(b), $l_{AB} = l_{CD} = \frac{\lambda}{2}$ and $l_{BC} = \frac{d_s}{2}$. The tortuosity can thence be obtained as:

$$\tau_{1-1} = \frac{l_{AB} + l_{BC} + l_{CD}}{l_{AB} + l_{CD}} = 1 + \frac{1}{2} \frac{d_s}{\lambda} = 1 + \frac{\sqrt{1 - \varepsilon}}{2} \quad (22)$$

Similarly, for streamline 2 in Fig. 2(b), as $l_{EF} = l_{GH} = l_{IJ} = l_{GI} = \frac{d_s}{2}$, $l_{FI} = \lambda - d_s$ and $l_{FG} = \sqrt{l_{GI}^2 + l_{FI}^2}$, the tortuosity is calculated as:

$$\begin{aligned} \tau_{1-2} &= \frac{l_{EF} + l_{FG} + l_{GH}}{l_{EF} + l_{FI} + l_{IJ}} = \frac{d_s + \sqrt{\left(\frac{d_s}{2}\right)^2 + (\lambda - d_s)^2}}{d} \\ &= \sqrt{1 - \varepsilon} + \frac{1}{2} \sqrt{9 - 5\varepsilon - 8\sqrt{1 - \varepsilon}} \end{aligned} \quad (23)$$

For the distribution of ligaments depicted in Fig. 2(b), the proportion of streamlines 1 and 2 is not affected by the porosity. No matter how the porosity changes in Fig. 2(b), the possibility of streamlines 1 and 2 is the same. Therefore, streamlines 1 and 2 in Fig. 2(b) have identical weight, e.g., $a_{1-1} = a_{1-2}$ and $a_{1-1} + a_{1-2} = 1$, so that the tortuosity can be obtained using a simple weighted average, as:

$$\begin{aligned} \tau_1 &= a_{1-1} \tau_{1-1} + a_{1-2} \tau_{1-2} = \frac{1}{2} \tau_{1-1} + \frac{1}{2} \tau_{1-2} \\ &= \frac{2 + 3\sqrt{1 - \varepsilon} + \sqrt{9 - 5\varepsilon - 8\sqrt{1 - \varepsilon}}}{4} \end{aligned} \quad (24)$$

where a_{1-1} is the weight value of streamline 1 and a_{1-2} is the weight value of streamline 2.

For streamline 1 in Fig. 2(d), its actual length l_{GH} is equal to the straight length of flow l_{GH} in the cell, yielding:

$$\tau_{2-1} = \frac{l_{GH}}{l_{GH}} = 1 \quad (25)$$

For streamline 2 in Fig. 2(d), since the boundary thickness is thin on ligament surface, the streamline of ligament boundary layer is thought to fit the ligament surface. Since $l_{MN} = l_{QR} = \frac{\lambda}{2}$, $l_{NO} = l_{PQ} = \frac{d_s}{2}$ and $l_{OP} = d_s$, the tortuosity can be calculated, as:

$$\tau_{2-2} = \frac{l_{MN} + l_{NO} + l_{OP} + l_{PQ} + l_{QR}}{l_{MN} + l_{OP} + l_{QR}} = \frac{\lambda + d_s}{\lambda} = 1 + \sqrt{1 - \varepsilon} \quad (26)$$

In Fig. 2(d), the streamline is tortuous near the ligament but almost straight away from it. As the porosity increases, the proportion of straight streamline increases while the proportion of tortuous streamline decreases. The two weights of streamlines in Fig. 2(d) are $a_{2-1} = \frac{\lambda^3 - \lambda d_s^2}{\lambda^3}$ and $a_{2-2} = \frac{\lambda d_s^2}{\lambda^3}$, yielding:

$$\begin{aligned} \tau_2 &= a_{2-1}\tau_{2-1} + a_{2-2}\tau_{2-2} = \left(\frac{\lambda^3 - \lambda d_s^2}{\lambda^3}\right)\tau_{2-1} + \frac{\lambda d_s^2}{\lambda^3}\tau_{2-2} \\ &= 1 + (1 - \varepsilon)\sqrt{1 - \varepsilon} \end{aligned} \quad (27)$$

Typically, in high porosity open-cell metallic foams, the pores are randomly distributed, with varying pore sizes. Consequently, proportions of the two ligament distributions in Fig. 2(a) and (c) cannot be directly measured. In this study, it is assumed that the two distributions have the same proportion, i.e., $a_1 = a_2 = \frac{1}{2}$, a_1 being the weight value for the dislocated and equidistant arrangement of Fig. 2(a) and a_2 the weight value for the square arrangement of Fig. 2(c). According to Eqs. (24) and (27), the average tortuosity can be finalized as:

$$\begin{aligned} \tau_{av} &= a_1\tau_1 + a_2\tau_2 = \frac{1}{2}\tau_1 + \frac{1}{2}\tau_2 \\ &= \frac{6 + (7 - 4\varepsilon)\sqrt{1 - \varepsilon} + \sqrt{9 - 5\varepsilon - 8\sqrt{1 - \varepsilon}}}{8} \end{aligned} \quad (28)$$

Finally, from Eqs. (12, 15-16) and (28), the fractal dimension of average tortuosity is obtained:

$$D_T = 1 + \frac{\ln \left\{ \frac{1}{8} \left[6 + (7 - 4\varepsilon)\sqrt{1 - \varepsilon} + \sqrt{9 - 5\varepsilon - 8\sqrt{1 - \varepsilon}} \right] \right\}}{\ln \left\{ \frac{\lambda_{\max}}{\lambda_{\min}} \frac{D_{f,3} - 1}{D_{f,3}} \left[\frac{\pi D_{f,3}}{6(3 - D_{f,3})} \frac{1 - \varepsilon}{\varepsilon} \right]^{\frac{1}{3}} \right\}} \quad (29)$$

For validating the tortuosity prediction, some classical models are referred to for comparison. When the porosity approaches 1, the average tortuosity also approaches 1, which is consistent with the actual physical meaning of tortuosity. As $\varepsilon = 0.95$, the current prediction is $\tau_{av} = 1.035$, which agrees well with the classical tortuosity predictions of 1.01-1.105 [30]. This confirms the fact that Eq. (28) can accurately predict the average tortuosity of metal foams at high porosity.

2.2.3. Maximum pore diameter

In the present model development, since the pores of varying sizes exhibit similar pore shapes, the maximum volume of a pore corresponds to the maximum size of a pore. In the RS shown in Fig. 1(d), the maximum pore diameter can be calculated from the maximum pore volume $V_{\max-pore}$ as:

$$\lambda_{\max} = \sqrt[3]{V_{\max-pore}} = \sqrt[3]{V_{total-pore} - V_{solid-pore}} = \sqrt[3]{V_{solid-pore}\varepsilon/(1 - \varepsilon)} \quad (30)$$

where $V_{total-pore}$ and $V_{solid-pore}$ are separately the total volume of pores and the volume of solid ligaments within the RS. The latter is given by:

$$V_{solid-pore} = 12 \cdot (\lambda - 2d_s)d_s^2 + 8d_s^3 = 12\lambda d_s^2 - 16d_s^3 \quad (31)$$

2.2.4. Shape factor G

In a previous fractal model [17], the cross-sectional shape of capillary tube is taken as circular. As for the current cubic RS proposed for open-cell metal foams, the capillary tube is assumed to have a square cross-section. Therefore, a dimensionless parameter – “shape factor” – is introduced to account for the influence of cross-sectional shape. Inspired by the models for accounting for the variation of metallic struts of metal foams, a shape factor for

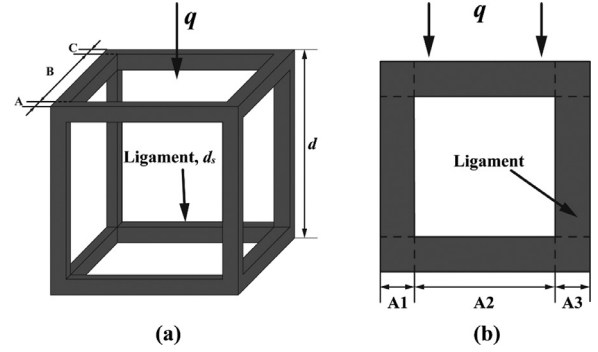


Fig. 3. Idealized pore structure model of open-cell metal foam: (a) representative structure (RS); (b) front view of the first layer of RS

considering the change of pore shape for metal foam is developed [8, 13, 31, 32]. With the cross-sectional area of capillary tube assumed to remain fixed along its length, the perimeter of its cross-section is an important parameter relating closely to its flow features. In the current study, with a circular capillary tube taken as reference, the square of the ratio of the perimeter of a circular cross-section to the perimeter of a cross-section having arbitrary shape is defined as the shape factor:

$$G = \left(\frac{P_{ref}}{P}\right)^2 \quad (32)$$

where P is perimeter of arbitrary cross section and P_{ref} represents the perimeter of a circle. When the cross-section is a square as considered in the present study, the shape factor is $G = \frac{\pi}{4}$ so that the original model of Eq. (8) is modified as:

$$K = G \frac{\pi}{128} \frac{L_0^{-1-D_T} D_f}{3 + D_T - D_f} \lambda_{\max}^{3+D_T} \quad (33)$$

2.2.5. Permeability formula

Finally, upon determining all the key parameters as detailed above, the permeability of open-cell metallic foam can be analytically obtained as:

$$\frac{K}{d_s^2} = G \frac{\pi}{128} \frac{D_{f,3}}{3 + D_T - D_{f,3}} \left[\frac{\pi D_{f,3}(1 - \varepsilon)}{6(3 - D_{f,3})\varepsilon} \right]^{-\frac{(1+D_T)}{3}} \left[\frac{\varepsilon}{1 - \varepsilon} \left(\frac{12}{\sqrt{1 - \varepsilon}} - 16 \right) \right]^{\frac{2}{3}} \quad (34)$$

where the fractal dimension of pore size distribution $D_{f,3}$ is calculated by Eq. (9) and the fractal dimension D_T by Eq. (29). Note that, contrary to previous permeability models, the current model of (24) does not contain any empirical or curve-fitting parameter. We turn next to establish a fractal model for effective thermal conductivity.

2.3. Fractal model of effective thermal conductivity

2.3.1. Thermal resistance of representative structure (RS)

In addition to permeability, the effective thermal conductivity of open-cell metallic foams is developed below using the fractal theory as well as the thermal-electrical analogy technique. Consider again the idealized cubic topology of Fig. 1(c) and its representative structure (RS) illustrated in Fig. 3(a). Let d denote the total length of the RS and let d_s represent the thickness of each ligament. With heat flow imposed on the top of the RS, heat conduction occurs mainly along the z -axis such that lateral thermal contact resistance can be safely neglected [33]. Therefore, thermal resistance along the direction of heat flow (z axis) needs only be considered. For conduction analysis, the effects of thermal radiation and convection in the RS are neglected.

In Fig. 3(a), the representative structure (RS) is divided into three parts A, B, and C from top to bottom. For part A, it is subdivided into three parts A1, A2 and A3 from left to right, where A1 and A3 have the same thermal resistance. The thermal resistance of A1 and A3 can be expressed as:

$$R_{A1} = R_{A3} = \frac{d}{k_s d_s^2} \quad (35)$$

Similarly, A2 thermal resistance can be obtained:

$$R_{A2} = \frac{2d_s}{k_s d_s (d - 2d_s)} + \frac{d - 2d_s}{k_f d_s (d - 2d_s)} \quad (36)$$

The thermal resistance A1, A2 and A3 can be connected in parallel to obtain the thermal resistance A, as expressed in Eq. (37).

$$\frac{1}{R_A} = \frac{1}{R_{A1}} + \frac{1}{R_{A2}} + \frac{1}{R_{A3}} = \frac{2k_s d_s^2}{d} + \frac{k_s k_f d_s (d - 2d_s)}{2k_f d_s + k_s (d - 2d_s)} \quad (37)$$

where k_f and k_s are the thermal conductivity of the liquid and solid phase, in respective. In a similar manner, the equivalent thermal resistance of the second layer and the third layer can be obtained, as:

$$\frac{1}{R_B} = \frac{1}{R_{B1}} + \frac{1}{R_{B2}} + \frac{1}{R_{B3}} = \frac{k_f (d - 2d_s)^2}{d} + \frac{2k_s k_f (d - 2d_s) d_s}{2d_s k_f + (d - 2d_s) k_s} \quad (38)$$

$$\frac{1}{R_C} = \frac{1}{R_{C1}} + \frac{1}{R_{C2}} + \frac{1}{R_{C3}} = \frac{2k_s d_s^2}{d} + \frac{k_s k_f (d - 2d_s) \lambda_s}{2\lambda_s k_f + (d - 2d_s) k_s} \quad (39)$$

The total thermal resistance of the cubic RS shown in Fig. 3(a) can thence be obtained as:

$$\frac{1}{R_{RS}} = \frac{1}{R_A} + \frac{1}{R_B} + \frac{1}{R_C} = d \left[4k_s \gamma^2 + k_f (1 - 2\gamma)^2 + \frac{4k_s k_f \gamma (1 - 2\gamma)}{2k_f \gamma + k_s (1 - 2\gamma)} \right] \quad (40)$$

where $d = \lambda + 2d_s$ and $\gamma = d_s/d$.

2.3.2. RS Chain model

Previously, when developing a thermal conductivity model for packed spherical particle beds, the heat conduction paths were described as multiple curved heat chains in parallel [19]. Each chain was composed of particles in close contact, as depicted schematically in Fig. 4(a). Built upon this concept, for the present idealized topological construction of open-cell metallic foams (Fig. 3), the conduction of heat along randomly-distributed RSs in close contact may be treated as heat flow along multiple RS chains in parallel; Fig. 4(b). We first derive the effective thermal conductivity of a single chain of RSs using the series model, and then use the parallel model to derive the effective conductivity of idealized open-cell metallic foam consisted of multiple RS chains having different pore sizes.

To begin with, we assume that the curved RS chains obey the fractal distribution law. As a curved chain of length $L_t(\lambda)$ contains $L_t(\lambda)/\lambda$ cubic RSs, according to the Fourier's law, its thermal resistance is:

$$R_{chain} = \frac{L_t(\lambda)}{\lambda} R_{RS} = \frac{\lambda^{-1-D_T} L_0^{D_T}}{(1+2\gamma)} \left[4k_s \gamma^2 + k_f (1 - 2\gamma)^2 + \frac{4k_s k_f \gamma (1 - 2\gamma)}{2k_f \gamma + k_s (1 - 2\gamma)} \right]^{-1} \quad (41)$$

Within the infinitesimal range of λ to $\lambda + d\lambda$ for pore sizes, the number of curved chains is $-dN$. These chains are connected in

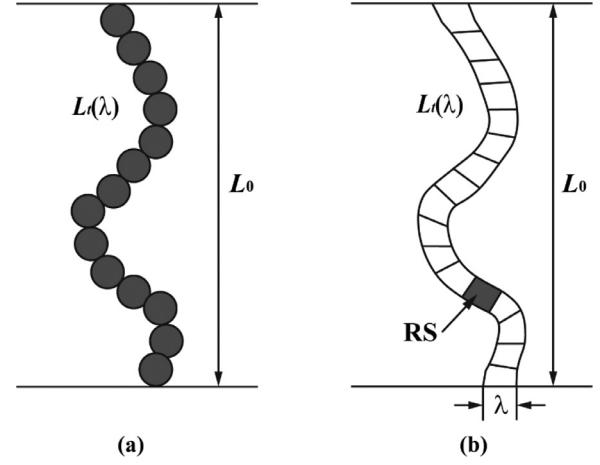


Fig. 4. Schematic of heat conduction path in a porous medium: (a) particle chain in packed spherical particle bed [19]; (b) solid ligament chain in open-cell metallic foam

parallel so that their total thermal resistance R_t can be obtained as:

$$\frac{1}{R_t} = \int_{\lambda_{min}}^{\lambda_{max}} \frac{D_{f,2} \lambda_{max}^{D_{f,2}} \lambda^{-(D_{f,2}+1)} d\lambda}{R_{chain}} \quad (42)$$

Fig. 1(c) depicts the minimal characteristic cubic cell for the open-cell metallic foam, which contains all the fractal pores, from smallest to largest size. The effective conductivity of the cube has the form of $k_e = \frac{L_0}{AR_t}$. From Eqs. (12), (14) and (42), the effective conductivity of the metallic foam consisted of multiple cubic RS chains can finally be obtained as:

$$k_e = \frac{(1+2\gamma)(2-D_{f,2})\varepsilon}{(D_T - D_{f,2} + 1)(1-\varepsilon)} \left[\frac{\pi D_{f,3}(1-\varepsilon)}{6(3-D_{f,3})\varepsilon} \right]^{\frac{1-D_T}{3}} \left(1 - \varepsilon^{\frac{D_T - D_{f,2} + 1}{2 - D_{f,2}}} \right) \times \left[4k_s \gamma^2 + k_f (1 - 2\gamma)^2 + \frac{4k_s k_f \gamma (1 - 2\gamma)}{2k_f \gamma + k_s (1 - 2\gamma)} \right] \quad (43)$$

where the fractal dimension D_T is determined by Eq. (29). With the porosity given by $\varepsilon = 1 - (V_s/V_{RS})$, its relationship with $\gamma = d_s/d$ can be obtained as:

$$\varepsilon = 1 - 12\gamma^2 + 16\gamma^3 \quad (44)$$

Again, note that, different from most existing models, the present model of Eq. (43) does not contain any empirical or curve-fitting parameter.

3. Results and discussion

3.1. Permeability

To validate the analytical fractal models developed in the previous sections for open-cell metallic foams, the model predictions are compared with not only existing experimental data [8, 25, 34-39] and simulated data [40, 41] (as summarized in Table 1), but also predictions obtained using alternative models proposed by other studies [6, 42-44]. Fig. 5 compares the present model predictions and the experimental data, which demonstrates satisfactory agreement between the two. By comparing with other permeability models for open-cell metallic foams [6, 42-44], it is indicated that the present fractal model exhibits a better agreement with experimental data. For instance, the validated porosity range is $0.61 < \varepsilon < 1.00$ for the Jackson-James model [43]; when the porosity drops below 0.61, the dimensionless permeability (K/d_s^2) is predicted to be negative; for the porosity range of $0.70 < \varepsilon < 1.00$, the

Table 1
Existing experimental and pore-scale simulation data of open-cell metal foams collected for comparison with the present analytical model.

References	PPI (Pores per inch ⁻¹)	Porosity, ε	Permeability $K \times 10^7$ (m ²)	d_s (mm)	d_p (mm)	K/d_p^2	K/d_s^2
Bhattacharya et al. [8] (Exp)	5	0.9726	2.7	0.5	4.02	0.017	1.080
	5	0.9118	1.8	0.55	3.8	0.012	0.595
	10	0.9486	1.2	0.4	3.13	0.012	0.750
	10	0.9138	1.1	0.45	3.28	0.010	0.543
	10	0.8991	0.94	0.43	3.2	0.009	0.508
	20	0.9546	1.3	0.3	2.7	0.018	1.444
	20	0.9245	1.1	0.35	2.9	0.013	0.898
	20	0.9005	0.9	0.35	2.58	0.014	0.735
	40	0.9659	0.55	0.2	1.9	0.015	1.375
	40	0.9272	0.61	0.25	2.02	0.015	0.976
	40	0.9132	0.53	0.2	1.8	0.016	1.325
	5	0.971	2.52	0.51	4	0.016	0.969
	5	0.946	2.17	0.47	3.9	0.014	0.982
	5	0.905	1.74	0.49	3.8	0.012	0.725
	10	0.949	1.49	0.37	3.1	0.016	1.088
	10	0.909	1.11	0.38	2.96	0.013	0.769
	20	0.978	1.42	0.38	2.8	0.018	0.983
	20	0.949	1.185	0.32	2.7	0.016	1.157
	20	0.906	0.854	0.34	2.6	0.013	0.739
	40	0.972	0.52	0.23	1.8	0.016	0.983
40	0.952	0.562	0.24	1.98	0.014	0.976	
40	0.937	0.568	0.24	2	0.014	0.986	
Phanikumar and Mahajan [25] (Exp)	5	0.899	1.989	0.5605	4.221	0.017	0.633
	5	0.93	2.069	0.5350	4.347	0.012	0.723
	10	0.9085	1.075	0.4428	3.422	0.012	0.548
	10	0.9386	1.171	0.4144	3.413	0.010	0.682
	20	0.92	1.063	0.3500	2.784	0.009	0.868
	20	0.9353	1.172	0.3321	2.723	0.018	1.063
	40	0.9091	0.5066	0.2500	1.935	0.013	0.811
	40	0.9586	0.5987	0.2094	1.727	0.014	1.365
Du Plessis et al. [34] (Exp)	N/A	0.973	0.0177 ^a	0.047	0.1265	0.015	0.801
	N/A	0.975	0.080 ^a	0.054	0.2609	0.015	2.743
	N/A	0.978	0.1603 ^a	0.054	0.3568	0.016	5.497
Mancin et al. [35] (Exp)	5	0.921	2.36	0.540	5.08	0.016	0.809
	10	0.903	1.90	0.529	2.54	0.014	0.679
	10	0.934	1.87	0.450	2.54	0.012	0.923
	10	0.956	1.82	0.445	2.54	0.016	0.919
	20	0.932	0.824	0.367	1.27	0.013	0.612
	40	0.930	0.634	0.324	0.635	0.018	0.604
Garrido et al. [36] (Exp)	10	0.818	0.2859	0.835	1.933	0.008	0.041
	20	0.804	0.0917	0.418	1.192	0.006	0.052
	30	0.816	0.0723	0.319	0.871	0.010	0.071
	45	0.813	0.0623	0.201	0.666	0.014	0.154
	10	0.852	0.395	0.88	2.252	0.008	0.051
	20	0.858	0.1466	0.451	1.131	0.011	0.072
	30	0.852	0.1107	0.33	0.861	0.015	0.102
	45	0.848	0.0995	0.206	0.687	0.021	0.234
Mancin et al. [37] (Exp)	20	0.930	0.535	0.315	1.175	0.014	0.539
	20	0.932	0.824	0.367	1.218	0.016	0.612
Hwang et al. [38] (Exp)	10	0.70	0.088	0.36	1.84	0.014	0.068
	10	0.80	0.2	0.36	1.92	0.020	0.154
	10	0.95	0.75	0.36	2.03	0.111	0.579
Wu et al. [39] (Exp)	N/A	0.55	0.0312	0.348 ^b	1.35	0.118	0.026 ^b
	N/A	0.7	0.0552	0.326 ^b	1.55	0.126	0.052 ^b
	N/A	0.85	0.103	0.203 ^b	1.35	0.009	0.250 ^b
	N/A	0.7	0.217	0.708 ^b	3.36	0.029	0.043 ^b
	N/A	0.7	0.303	0.946 ^b	4.49	0.029	0.034 ^b
Zafari et al. [40] (Sim)	N/A	0.96	0.94	0.243	2	0.024	2.514 ^b
	N/A	0.96	4.71	0.486	4	0.029	3.149 ^b
	N/A	0.96	5.39	0.730	6	0.015	1.602 ^b
Krishman et al. [41] (Sim)	N/A	0.945	N/A	N/A	N/A	0.014	1.242 ^b
	N/A	0.953	N/A	N/A	N/A	0.014	1.419 ^b

Note: "Exp" and "Sim" represent experimental data and simulated data, respectively.

^a Permeability is calculated by [34]: $K = \frac{d^2 \varepsilon^3}{36\tau(\tau-1)}$

^b Calculated based on empirical correlation [8, 45]: $\frac{d_s}{d_p} = 1.18 \sqrt{\frac{1-\varepsilon}{3\pi}} \left(\frac{1}{1-e^{-(1-\varepsilon)/0.04}} \right)$

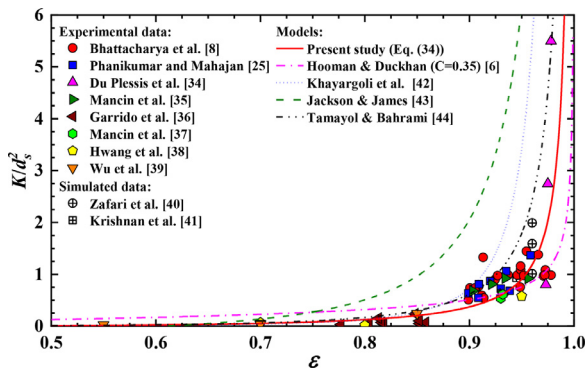


Fig. 5. Comparison between model predictions and experimental data for open-cell metallic foams [6, 8, 25, 34-44]

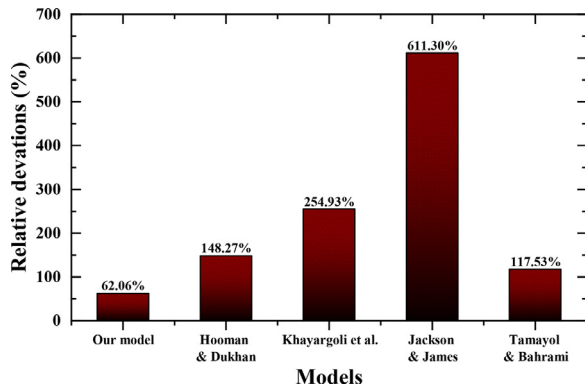


Fig. 6. Comparison of average RDs among various permeability models for open-cell metallic foams

model significantly overestimates the permeability. Similarly, for the porosity range of $0.50 < \epsilon < 0.85$, the Hooman-Dukhan model overestimates the permeability. As can be seen from Fig. 5, the proposed fractal model predicts the variation trend of permeability more accurately over the entire porosity range considered.

For quantitative comparison, relative deviation (RD) is applied to evaluate different permeability models, which is defined by:

$$RD = \left| \frac{\left(\frac{K}{d_s^2}\right)_{pre} - \left(\frac{K}{d_s^2}\right)_{exp}}{\left(\frac{K}{d_s^2}\right)_{exp}} \right| \quad (45)$$

where the subscripts “exp” and “pre” denote separately experimental measurement and model prediction.

Fig. 6 compares the values of RD calculated using different permeability models. Among the existing models considered, the Jackson-James model has the largest RD (611.30%), while the Hooman-Dukhan model has the smallest RD (148.27%). In contrast, achieving a RD of only 62.06%, the present fractal permeability model improves the RD by 58.14% relative to the Hooman-Dukhan model. This not only indicates the applicability and feasibility of our model, but also demonstrates that fractal theory can be employed to study transport properties of open-cell metallic foams. The main reason for the superior prediction accuracy of the proposed fractal model is that traditional geometric analysis methods use a periodic unit cell (UC) to characterize the random pore structure of open-cell metal foam, thus ignoring the typically randomness of its pore distribution. In contrast, with the effect of pore distribution randomness duly considered, the present fractal model is capable of predicting the variation trend of foam permeability with porosity in a wide range ($0.55 < \epsilon < 0.98$). It needs to be emphasized here that the proposed analytical model, i.e., Eq. (34),

Table 2

Relative deviations (RDs) between permeability models and experimental data.

Models	RD ranges	MAPEs (averaged RDs)
Present study	0.08-712.84%	62.06%
Hooman and Dukhan [6]	0.35-1975.88%	148.27%
Khayargoli et al. [42]	0.35-1865.40%	254.93%
Jackson and James [43]	96.60-3197.21%	611.30%
Tamayol and Bahrami [44]	2.55-993.36%	117.53%

does not contain any empirical or fitting parameter, except that assuming a fixed ratio of minimum pore diameter to maximum pore diameter (i.e., $\lambda_{min}/\lambda_{max} = 0.001$). Further, each parameter of the model, including D_f , D_T , ϵ and τ_{av} , has a clear physical meaning. It should be noted here that the experimental data for metal foam permeability have strong diversity and divergence, since they are measured based on different kinds of metal foams with various pore shapes and diameter distributions. Therefore, the permeability predicted by the models will bring huge deviation due to individual data points. It is inadequate to judge a model only according to the relative deviation (RD) and the Mean Absolute Percentage Error (MAPE) [21, 22] (see Table 2). The MAPE is defined by:

$$MAPE = \frac{1}{m} \sum_{n=1}^m \left| \frac{\left(\frac{K}{d_s^2}\right)_{pre,n} - \left(\frac{K}{d_s^2}\right)_{exp,n}}{\left(\frac{K}{d_s^2}\right)_{exp,n}} \right| \quad (46)$$

where m is the number of experimental data. One should select a proper model according to the specific porosity range when predicting permeability.

Permeability is a property that describes the easiness of fluid through open porous media. For Darcy flow, the pressure drop can be determined by

$$-\frac{dp}{dl} = \frac{\mu u}{K} \quad (47)$$

where dp/dl is the pressure drop along the nominal flow direction, μ is the dynamic viscosity, and u is the mean velocity along the flow direction. If permeability of a porous medium is given, the corresponding pressure drop within Darcy flow regime can be readily calculated by Eq. (47). For other conditions of non-Newtonian fluids or fluids in high velocity regime, Darcy’s law is not satisfied. However, for Newtonian fluids in a high velocity regime, if permeability K and inertia coefficient f are determined, its pressure drop can be also calculated by

$$-\frac{\Delta p}{\Delta l} = \frac{\mu u}{K} + \frac{\rho f}{\sqrt{K}} u^2 \quad (48)$$

where f is the inertia coefficient and ρ is the density, and the K in Eq. (48) is the permeability for porous media in Darcy flow regime.

3.2. Effective thermal conductivity

For the effective thermal conductivity of open-cell metallic foams saturated with air, water or paraffin, Fig. 7 compares predictions obtained using the present model and existing models [11-13, 15, 46-48] and existing experimental data (details summarized in Table 3), respectively. The model predictions are carried out using materials properties shown in Table 4. As seen, the effective conductivity decreases, nearly linearly, with increasing porosity. Regardless of the type of saturating fluid (air, water or paraffin) or material make (aluminum, copper or nickel), predictions of the present model agree quite well with experimental data, the Boomsma-Poulikakos model overestimates, while the model of Yang et al. [46] underestimates. Interestingly, relative to

Table 3

Experimental and pore-scale simulation data of effective thermal conductivity for open-cell aluminum (Al), copper (Cu) and Nickel (Ni) foams saturated with air, water or paraffin.

References	PPI (Pores per inch ⁻¹)	Porosity, ε	$k_{e,air}$ [W/(m-K)]	Remarks		
Yao et al. [13]	10	0.925	11.16	Cu-air (Exp)		
	10	0.935	9.71			
	10	0.941	8.12			
	20	0.895	17.68			
	20	0.906	16.52			
	20	0.912	12.61			
	20	0.914	13.62			
	20	0.918	12.61			
	20	0.926	12.61			
	20	0.932	10.43			
	20	0.937	8.70			
	20	0.942	9.13			
	20	0.968	4.64			
	20	0.973	3.91			
	20	0.975	3.62			
	20	0.975	3.48			
	20	0.978	3.04			
	40	0.926	12.32			
	40	0.935	9.57			
	40	0.945	8.41			
Yao et al. [13]	20	0.914	14.10	Cu-water (Exp)		
	20	0.937	9.33			
	20	0.975	4.03			
Yao et al. [13]	20	0.914	13.78	Cu-paraffin (Exp)		
	20	0.937	8.80			
	20	0.975	3.71			
Yang et al. [14]	5	0.913	6.63	Al-air (Exp)		
	6	0.953	3.34			
	7	0.912	6.72			
	8	0.957	3.57			
	10	0.917	6.63			
	10	0.928	5.63			
	13	0.963	2.88			
	20	0.923	5.81			
	Yang et al. [14]	5	0.913		7.91	Al-water (Exp)
		6	0.953		4.94	
7		0.912	8.01			
8		0.957	4.71			
10		0.917	7.91			
10		0.928	6.95			
13		0.963	4.12			
20		0.923	7.04			
Phanikumar and Mahajan [25]	N/A	0.899	7.733	Al-air (Exp)		
	N/A	0.93	5.357			
	N/A	0.9085	7.008			
	N/A	0.9386	4.711			
	N/A	0.92	6.13			
	N/A	0.9353	4.963			
	N/A	0.9091	6.963			
Calmidi and Mahajan [48]	N/A	0.9586	3.185	Al-air (Exp)		
	5	0.971	2.7			
	5	0.946	4.6			
	5	0.905	6.7			
	10	0.949	4			
	10	0.909	6.7			
	20	0.978	2.2			
	20	0.949	3.9			
	20	0.906	6.9			
	40	0.972	2.5			
	40	0.952	3.9			
	40	0.937	4.5			
	Calmidi and Mahajan [48]	5	0.971		3.7	Al-water (Exp)
5		0.946	5.4			
5		0.905	7.65			
10		0.949	4.95			
10		0.909	7.6			
20		0.978	3.05			
20		0.949	4.8			
20		0.906	7.65			
40		0.972	3.3			
40		0.952	4.75			
40		0.937	5.35			
Dyga and Witzak [49]		40	0.929	5.48	Al-air (Exp)	

(continued on next page)

Table 3 (continued)

Dyga and Witczak [49]	40	0.929	5.64	Al-water (Exp)
	40	0.929	6.36	
	40	0.929	6.82	
Sadeghi et al. [50]	10	0.903	7.36	Al-air (Exp)
	10	0.945	4.54	
	20	0.906	6.86	
	20	0.953	3.79	
Bianchi et al. [51]	10	0.897	7.7	Al-air (Sim)
	40	0.890	7.2	
	40	0.950	3.9	
Schmierer et al. [52]	20	0.95	3.5	Al-air (Exp)
Schmierer et al. [52]	20	0.95	4.873	Al-water (Exp)
Schmierer and Razani [53]	5	0.92	6.3	Al-water (Exp)
	10	0.886	10.2	
	10	0.962	3.12	
	20	0.915	7.32	
	30	0.913	7.4	
Xiao et al. [54]	N/A	0.9717	1.31	Ni-paraffin (Exp)
	N/A	0.9728	1.23	
	N/A	0.9765	0.98	

Note: The abbreviations of “Exp” and “Sim” represent experiment and simulation data in this Table.

experimental data, the Zenner-Edouard model predicts lower conductivities at $\varepsilon < 0.96$ but higher ones at $\varepsilon > 0.96$. The other models proposed by Dai et al. [12], Yao et al. [13], and Wu and Huang [15] can correctly predict the variation trend effective thermal conductivity with porosity for open-cell metallic foams saturated with

different fluids. Note that, Dai et al. [12] made modifications to inclined ligaments in the tetrakaidecahedron geometry proposed by Boomsma and Polulikakos [11-13, 15, 46-48] for metal foams. Although the prediction accuracy of Dai et al.’s model is much higher than the Boomsma-Polulikakos model, it still slightly overestimates

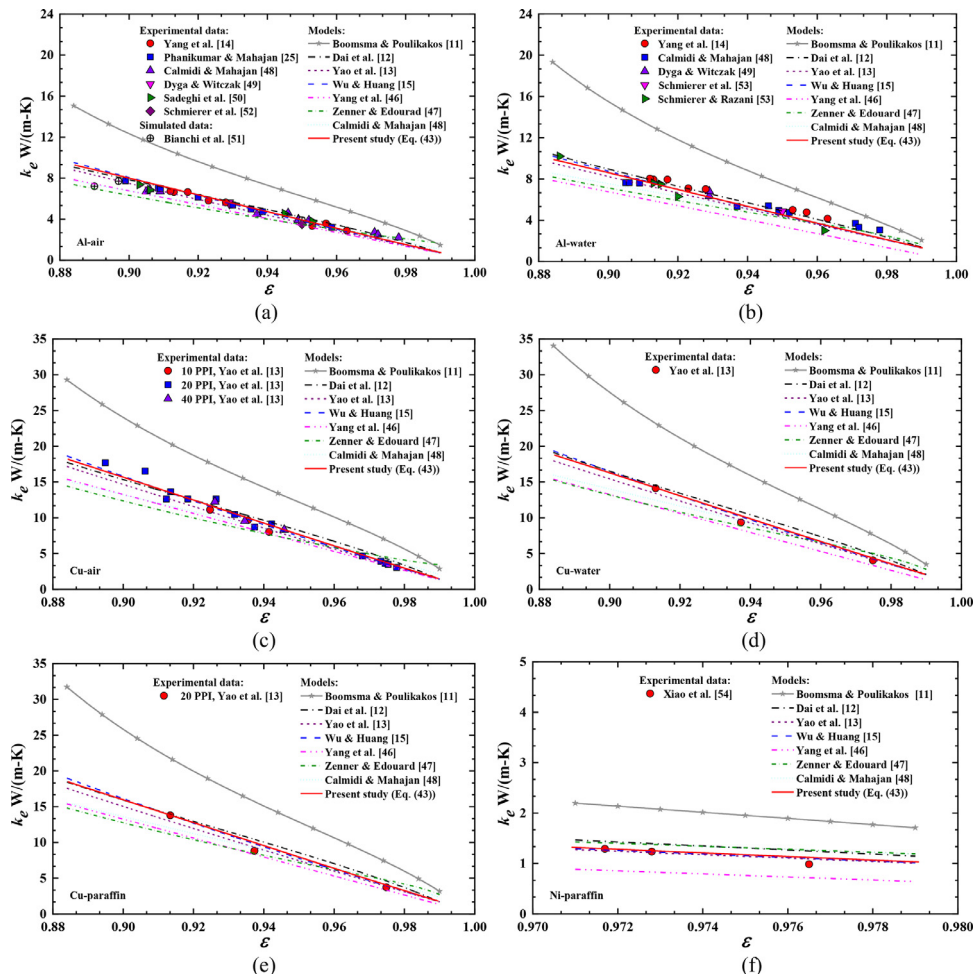


Fig. 7. Comparisons between predictions obtained with effective conductivity models and existing experimental data: (a) air-saturated Al (aluminum) foam [11-15, 25, 46-52]; (b) water-saturated Al foam [11-15, 46-49, 52, 53]; (c) air-saturated Cu (copper) foam [11-13, 15, 46-48]; (d) water-saturated Cu foam [11-13, 15, 46-48]; (e) paraffin-saturated Cu foam [11-13, 15, 46-48]; and (f) paraffin-saturated Ni (nickel) foam [11-13, 15, 46-48, 54]

Table 4
Material thermal conductivities used for analytical model prediction.

Materials	k (W/(m-K))	Materials	k (W/(m-K))
Aluminum	203	Air	0.026
Copper	398	Water	0.598
Nickle	91.4	Paraffin	0.305

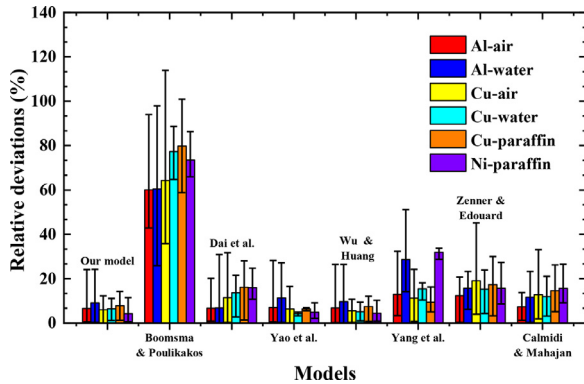


Fig. 8. Comparison of RDs for different metal foams at high porosities

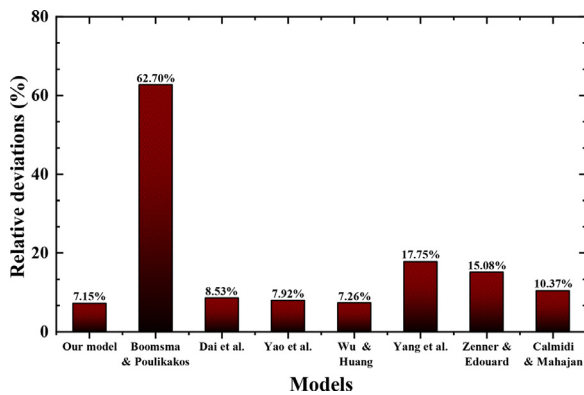


Fig. 9. Comparison of average RDs calculated with different effective conductivity models at high porosities

the effective conductivity of copper and nickel foams for porosities higher than 0.91, as shown in Fig. 7(c)-(f). Overall, for the porosity range of 0.88 to 1.0, the predictions obtained using the models of Yao et al. [13] and Wu and Huang [15] exhibit reasonable agreement with experimental data.

Similar to the case of permeability, Fig. 8 compares the values of RD calculated by comparing with experimental data in each source. It is seen that our model gives better predictions compared with other models. For air- and water-saturated Al foams, the RD s of our model are lower than those of the Wu-Huang model, the latter being the best among existing models considered. For paraffin-saturated Ni foams, our model presents lower RD s than other models as well. More detailed values for RD are summarized in Table 5.

Upon averaging all the RD values for each model, Fig. 9 compares the average RD s calculated with different models. As seen, with an average deviation of 7.15%, our model presents the smallest RD among all the models considered, followed by the Wu-Huang model (7.26%), the Yao et al. model (7.92%), the Dai et al. model (8.53%), the Calmidi-Mahajan model (10.37%), the Zenner-Edouard model (15.08%), the Yang et al. model (17.75%), and the Boomsma-Poulidakos model (62.70%). It should be noted here that although the Calmidi-Mahajan model exhibits a relatively low RD , it is de-

Table 5
Relative deviations (RD s) between effective conductivity models and experimental data.

Samples	Models	RD ranges	Average RD s
Al-air	Present study	0.43-24.10%	6.62%
	Boomsma and Poulidakos [11]	42.83-94.01%	60.09%
	Dai et al. [12]	0.86-20.17%	6.66%
	Yao et al. [13]	0.44-28.23%	6.99%
	Wu and Huang [15]	0.22-26.40%	6.80%
	Yang et al. [46]	3.33-32.33%	12.96%
	Zenner and Edouard [47]	0.30-20.68%	12.38%
	Calmidi and Mahajan [48]	1.16-13.77%	7.33%
Al-water	Present study	0.25-24.19%	9.06%
	Boomsma and Poulidakos [11]	25.83-97.92%	60.44%
	Dai et al. [12]	0.09-30.91%	6.79%
	Yao et al. [13]	0.30-27.18%	11.24%
	Wu and Huang [15]	0.071-26.39%	9.64%
	Yang et al. [46]	14.07-51.19%	28.56%
	Zenner and Edouard [47]	6.10-23.26%	15.65%
	Calmidi and Mahajan [48]	0.29-23.25%	11.62%
Cu-air	Present study	0.04-12.26%	5.98%
	Boomsma and Poulidakos [11]	35.72-114.01%	64.29%
	Dai et al. [12]	0.27%-31.71%	11.48%
	Yao et al. [13]	0.07-16.54%	6.31%
	Wu and Huang [15]	0.32-10.69%	5.54%
	Yang et al. [46]	0.74-24.18%	11.17%
	Zenner and Edouard [47]	3.96-45.15%	19.04%
	Calmidi and Mahajan [48]	1.80-33.13%	12.78%
Cu-water	Present study	1.07-11.06%	6.40%
	Boomsma and Poulidakos [11]	64.70-88.65%	77.27%
	Dai et al. [12]	2.76-21.56%	13.65%
	Yao et al. [13]	3.21-4.91%	4.22%
	Wu and Huang [15]	0.96-9.42%	5.13%
	Yang et al. [46]	10.41-18.14%	15.40%
	Zenner and Edouard [47]	4.35-23.93%	15.33%
	Calmidi and Mahajan [48]	3.09-21.09%	11.93%
Cu-paraffin	Present study	1.15-14.21%	7.76%
	Boomsma and Poulidakos [11]	58.77-100.98%	79.74%
	Dai et al. [12]	1.41-28.03%	16.18%
	Yao et al. [13]	5.51-6.87%	6.33%
	Wu and Huang [15]	0.75-12.11%	7.39%
	Yang et al. [46]	5.01-16.25%	9.43%
	Zenner and Edouard [47]	3.19-30.02%	17.35%
	Calmidi and Mahajan [48]	5.09-26.20%	14.57%
Ni-paraffin	Present study	0.54-11.46%	4.24%
	Boomsma and Poulidakos [11]	65.94-86.21%	73.49%
	Dai et al. [12]	10.76-24.72%	15.96%
	Yao et al. [13]	2.11-9.04%	4.90%
	Wu and Huang [15]	0.79-10.23%	4.40%
	Yang et al. [46]	28.74-33.72%	31.92%
	Zenner and Edouard [47]	8.63-27.31%	15.67%
	Calmidi and Mahajan [48]	9.03-26.49%	15.59%

veloped by assuming that the open-cell metallic foam has a two-dimensional cellular morphology.

The effective thermal conductivity model developed herein based on fractal theory is in good agreement with experimental data, demonstrating again the applicability of fractal theory in heat transfer studies of open-cell metallic foams. Further, the model built upon fractal theory contains no empirical or curve-fitting parameter, and each parameter appearing in the model has a specific physical meaning. Compared with existing models, the present model more clearly reveals key factors that affect the effective thermal conductivity and the related physical mechanisms. The developed fractal model considers the randomness of pore size and distribution, consistent with such randomness observed in real metallic foams.

4. Conclusion

The fractal theory has been employed to characterize the randomly distributed pores in open-cell metallic foams and then to

establish analytical models for predicting both the permeability and effective thermal conductivity. The following conclusions can be drawn.

- (1) For modelling permeability: with the cellular foam morphology characterized using fractal dimensions, the permeability is analytically expressed as a function of porosity, average tortuosity, and pore size distribution, with no empirical or fitting parameter needed in contrast to previous permeability models.
- (2) The permeability model predictions compare well with existing experimental data for foam porosities varying over a wide range (from 0.55 to 0.98). Relative to existing analytical models, the current model exhibits the smallest relative deviations (62.06%) from experimental data; while the relative deviations for the previous models range from 117.53%–611.30% for the wide porosity range.
- (3) For modelling conductivity: the effective thermal conductivity is analytically expressed as a function of porosity, thermal conductivity of the material makes of the foam and that of the filling medium, average tortuosity, and pore size distribution, with no empirical or fitting parameter needed in contrast to previous effective thermal conductivity models.
- (4) Compared with existing effective conductivity models, the present model exhibits good accuracy (relative deviation 7.15% from experimental data) for high-porosity (0.88–0.99) aluminum, copper and nickel foams saturated with air, water or paraffin. In our model, the RDs of Al-air, Al-water, Cu-air, Cu-water, Cu-paraffin and Ni-paraffin are 6.62%, 9.06%, 11.24%, 5.98%, 6.40%, 7.76% and 4.24%, in respectively.

Declaration of Competing Interest

The authors declare that they have no known competing financial interests or personal relationships that could have appeared to influence the work reported in this paper.

CRediT authorship contribution statement

Tian Xiao: Software, Formal analysis, Writing – original draft. **Xiaohu Yang:** Conceptualization, Methodology, Writing – original draft, Supervision. **Kamel Hooman:** Supervision, Writing – review & editing. **Tian Jian Lu:** Supervision, Writing – review & editing.

Acknowledgements

This work was supported by the National Natural Science Foundation of China (51976155, 12032010), the Fundamental Research Funds for Central Universities (xtr042019019), and the Open Fund of the State Key Laboratory of Mechanics and Control of Mechanical Structures (MCMS-E0219K02, MCMS-I-0219K01). One of the authors (Xiaohu Yang) gratefully acknowledged the support of K. C. Wong Education Foundation.

Reference

- [1] N Bianco, M Iasiello, GM Mauro, L Pagano, Multi-objective optimization of finned metal foam heat sinks: Tradeoff between heat transfer and pressure drop, *Appl. Therm. Eng.* 182 (2021) 116058.
- [2] M Iasiello, M Mameli, S Filipposchi, N. Bianco, Metal foam/PCM melting evolution analysis: Orientation and morphology effects, *Appl. Therm. Eng.* 187 (2021) 116572.
- [3] S Mancin, A Diani, L Doretti, K Hooman, L. Rossetto, Experimental analysis of phase change phenomenon of paraffin waxes embedded in copper foams, *Int. J. Therm. Sci.* 90 (2015) 79–89.
- [4] XH Yang, JF Guo, B Yang, HN Cheng, P Wei, YL He, Design of non-uniformly distributed annular fins for a shell-and-tube thermal energy storage unit, *Appl. Energy* 279 (2020) 15772.
- [5] G Junfei, L Zhan, D Zhao, Y Jiabang, Y Xiaohu, Y. Jinyue, Effect of fin-metal foam structure on thermal energy storage: an experimental study, *Renewable Energy* 172 (2021) 57–72.
- [6] K Hooman, N. Dukhan, A theoretical model with experimental verification to predict hydrodynamics of foams, *Transp. Porous Media* 100 (2013) 393–406.
- [7] Z Hashin, S. Shtrikman, A variational approach to the theory of the effective magnetic permeability of multiphase materials, *J. Appl. Phys.* 33 (1962) 3125–3131.
- [8] A Bhattacharya, VV Calmidi, RL Mahajan, Thermophysical properties of high porosity metal foams, *Int. J. Heat Mass Transfer* 45 (2002) 1017–1031.
- [9] TT Huu, M Lacroix, CP Huu, D Schweich, D Edouard, Towards a more realistic modeling of solid foam: Use of the pentagonal dodecahedron geometry, *Chem. Eng. Sci.* 64 (2009) 5131–5142.
- [10] V Calmidi, R. Mahajan, Forced convection in high porosity metal foams, *J. Heat Transfer* 122 (2000) 557–565.
- [11] K Boomsma, D Poulikakos, Corrigendum for the paper: K. Boomsma, D. Poulikakos, "On the effective thermal conductivity of a three-dimensionally structured fluid-saturated metal foam" [*International Journal of Heat and Mass Transfer*, 44 (2001) 827–836], *Int. J. Heat Mass Transfer* 54 (2011) 746–748.
- [12] Z Dai, K Nawaz, YG Park, J Bock, AM. Jacobi, Correcting and extending the Boomsma–Poulikakos effective thermal conductivity model for three-dimensional, fluid-saturated metal foams, *Int. Commun. Heat Mass Transfer* 37 (2010) 575–580.
- [13] Y Yao, H Wu, Z. Liu, A new prediction model for the effective thermal conductivity of high porosity open-cell metal foams, *Int. J. Therm. Sci.* 97 (2015) 56–67.
- [14] X Yang, J Bai, H Yan, J Kuang, T. Kim, An Analytical Unit Cell Model for the Effective Thermal Conductivity of High Porosity Open-Cell Metal Foams, *Transp. Porous Media* 102 (2014) 403–426.
- [15] D Wu, C. Huang, Thermal conductivity model of open-cell foam suitable for wide span of porosities, *Int. J. Heat Mass Transfer* 130 (2019) 1075–1086.
- [16] B Yu, J. Li, Some fractal characters of porous media, *Fractals* 9 (2001) 365–372.
- [17] B Yu, P. Cheng, A fractal permeability model for bi-dispersed porous media, *Int. J. Heat Mass Transfer* 45 (2002) 2983–2993.
- [18] J Cai, L Luo, RAN Ye, X Zeng, X. Hu, Recent advances on fractal modeling of permeability for fibrous porous media, *Fractals* 23 (2015) 1540006.
- [19] B Yu, P. Cheng, Fractal Models for the Effective Thermal Conductivity of Bidispersed Porous Media, *J. Thermophys. Heat Transfer* 16 (2002) 22–29.
- [20] X Yang, TJ Lu, T. Kim, An analytical model for permeability of isotropic porous media, *Phys. Lett. A* 378 (2014) 2308–2311.
- [21] M Iasiello, N Bianco, WKS Chiu, V. Naso, Thermal conduction in open-cell metal foams: anisotropy and representative volume element, *Int. J. Therm. Sci.* 137 (2019) 399–409.
- [22] M Iasiello, N Bianco, WKS Chiu, V. Naso, Anisotropic convective heat transfer in open-cell metal foams: assessment and correlations, *Int. J. Heat Mass Transfer* 154 (2020) 119682.
- [23] Benoit B Mandelbrot, *The Fractal Geometry of Nature*, WH freeman, New York, 1982.
- [24] A Majumdar, B. Bhushan, Role of Fractal Geometry in Roughness Characterization and Contact Mechanics of Surfaces, *J. Tribol.* (1990).
- [25] MS Phanikumar, RL Mahajan, Non-Darcy natural convection in high porosity metal foams, *Int. J. Heat Mass Transfer* 45 (2002) 3781–3793.
- [26] B. Yu, Analysis of flow in fractal porous media, *Appl. Mech. Rev.* 61 (2008) 050801.
- [27] B. Yu, Fractal character for tortuous streamtubes in porous media, *Chin. Phys. Lett.* 22 (2005) 158.
- [28] FA. Dullien, *Porous media: fluid transport and pore structure*, Academic press, 2012.
- [29] M Yun, B Yu, P Xu, J. Wu, Geometrical Models for Tortuosity of Streamlines in Three-Dimensional Porous Media, *Can. J. Chem. Eng.* 84 (2006) 301–309.
- [30] L Shen, ZX. Chen, Critical review of the impact of tortuosity on diffusion, *Chem. Eng. Sci.* 62 (2007) 3748–3755.
- [31] G Ambrosio, N Bianco, WKS Chiu, M Iasiello, V Naso, M. Oliviero, The effect of open-cell metal foams strut shape on convection heat transfer and pressure drop, *Appl. Therm. Eng.* 103 (2016) 333–343.
- [32] P De Jaeger, C T'Joer, H Huisseune, B Arneel, M De Paepe, An experimentally validated and parameterized periodic unit-cell reconstruction of open-cell foams, *J. Appl. Phys.* 109 (2011) 103519.
- [33] Y Ma, B Yu, D Zhang, M. Zou, A self-similarity model for effective thermal conductivity of porous media, *J. Phys. D Appl. Phys.* 36 (2003) 2157.
- [34] P Du Plessis, A Montillet, J Comiti, J. Legrand, Pressure drop prediction for flow through high porosity metallic foams, *Chem. Eng. Sci.* 49 (1994) 3545–3553.
- [35] S Mancin, C Zilio, A Cavallini, L. Rossetto, Pressure drop during air flow in aluminum foams, *Int. J. Heat Mass Transfer* 53 (2010) 3121–3130.
- [36] GI Garrido, F Patcas, S Lang, B. Kraushaar-Czarnetzki, Mass transfer and pressure drop in ceramic foams: a description for different pore sizes and porosities, *Chem. Eng. Sci.* 63 (2008) 5202–5217.
- [37] S Mancin, C Zilio, L Rossetto, A. Cavallini, Foam height effects on heat transfer performance of 20 ppi aluminum foams, *Appl. Therm. Eng.* 49 (2012) 55–60.
- [38] J-J Hwang, G-J Hwang, R-H Yeh, C-H. Chao, Measurement of interstitial convective heat transfer and frictional drag for flow across metal foams, *J. Heat Transfer* 124 (2002) 120–129.
- [39] Z Wu, C Caliot, F Bai, G Flamant, Z Wang, J Zhang, et al., Experimental and numerical studies of the pressure drop in ceramic foams for volumetric solar receiver applications, *Appl. Energy* 87 (2010) 504–513.
- [40] M Zafari, M Panjepour, M Meratian, MD. Emami, CFD simulation of forced convective heat transfer by tetrakaidehedron model in metal foams, *J. Porous Media* 19 (2016).

- [41] S Krishnan, JY Murthy, SV. Garimella, Direct simulation of transport in open-cell metal foam, *J. Heat Transfer* 128 (2006) 793–799.
- [42] P Khayargoli, V Loya, L Lefebvre, M. Medraj, The impact of microstructure on the permeability of metal foams, *CSME Forum* 2004 (2004) 220–228.
- [43] GW Jackson, DF. James, The permeability of fibrous porous media, *Can. J. Chem. Eng.* 64 (1986) 364–374.
- [44] A Tamayol, M. Bahrani, Transverse permeability of fibrous porous media, *Phys. Rev. E Stat. Nonlin Soft Matter Phys.* 83 (2011) 046314.
- [45] Calmidi VV. *Transport phenomena in high porosity fibrous metal foams*. 1999.
- [46] X Yang, J Kuang, T Lu, F Han, T. Kim, A simplistic analytical unit cell based model for the effective thermal conductivity of high porosity open-cell metal foams, *J. Phys. D Appl. Phys.* 46 (2013) 255302.
- [47] A Zenner, D. Edouard, Revised cubic model for theoretical estimation of effective thermal conductivity of metal foams, *Appl. Therm. Eng.* 113 (2017) 1313–1318.
- [48] V.V Calmidi, R.L. Mahajan, The Effective Thermal Conductivity of High Porosity Fibrous Metal Foams, *J. Heat Transfer* (1999).
- [49] R Dyga, S. Witczak, Investigation of Effective Thermal Conductivity Aluminum Foams, *Procedia Eng.* 42 (2012) 1088–1099.
- [50] E Sadeghi, S Hsieh, M. Bahrani, Thermal conductivity and contact resistance of metal foams, *J. Phys. D Appl. Phys.* 44 (2011) 125406.
- [51] E Bianchi, T Heidig, CG Visconti, G Groppi, H Freund], An appraisal of the heat transfer properties of metallic open-cell foams for strongly exo-/endo-thermic catalytic processes in tubular reactors, *Chem. Eng. J.* 198 (2012) 512–528.
- [52] EN Schmierer, J Paquette, A Razani, KJ. Kim, Effective thermal conductivity of fully-saturated high porosity metal foam, *ASME Heat Transf./Fluids Eng. Summer Conf.* 46903 (2004) 229–237.
- [53] EN Schmierer, A. Razani, Self-consistent open-celled metal foam model for thermal applications, *J. Heat Transfer* 128 (2006) 1194–1203.
- [54] X Xiao, P Zhang, M. Li, Effective thermal conductivity of open-cell metal foams impregnated with pure paraffin for latent heat storage, *Int. J. Therm. Sci.* 81 (2014) 94–105.